

Structure and energetics of ammonia clusters (NH₃)_n (n=3-20) investigated using a rigid-polarizable model derived from *ab initio* calculations.

Journal:	<i>The Journal of Physical Chemistry</i>
Manuscript ID:	jp-2007-106796.R1
Manuscript Type:	Article
Date Submitted by the Author:	11-Jan-2008
Complete List of Authors:	Mella, Massimo; Cardiff University, School of Chemistry Curotto, Emanuele; Arcadia University Janeiro-Barral, Paula; Cardiff University, School of Chemistry



1
2
3
4
5
6
7
8 Structure and energetics of ammonia clusters $(\text{NH}_3)_n$ ($n = 3 - 20$)
9
10
11 investigated using a rigid-polarizable model derived from *ab initio*
12
13
14
15 calculations.
16
17

18 Paula E. Janeiro-Barral and Massimo Mella*

19
20 School of Chemistry, Cardiff University,
21
22 Main Building, Park Place, Cardiff CF10 3AT (UK),
23
24

25 Electronic mail: mellam@cardiff.ac.uk
26

27
28 E. Curotto

29
30 Department of Chemistry and Physics,
31
32 Arcadia University,
33
34 Glenside, Pennsylvania 19038
35

36 Electronic mail:
37

38 January 11, 2008
39
40
41

42 Abstract

43
44 An analytical model has been developed to describe the interaction between rigid ammonia molecules
45 including the explicit description of induction. The parameters of the model potential were chosen by
46 fitting high quality *ab initio* data obtained using second order Møller-Plesset (MP2) perturbation theory
47 and extended basis sets. The description of polarization effects is introduced by using a non-iterative form
48 of the “charge on spring model”, the latter accounting for more than 95% of the dipole induction energy and
49 of the increased molecular dipole. Putative global minima for $(\text{NH}_3)_n$ ($n=3-20$) have been optimized using
50 this new model, the structure and energetics of the clusters with $n=3-5$ being found in good agreement with
51 previous *ab initio* results including electronic correlation. Results for larger species have been compared
52 with previous structural studies where only non-polarizable models were employed. Our model predicts
53 larger binding energies for any cluster size than previous analytical surfaces, the results often suggesting a
54
55
56
57
58
59
60

1
2
3 reorganization of the relative energy ranking and a different structure for the global minimum.
4
5
6
7
8
9
10
11
12
13
14
15
16
17
18
19
20
21
22
23
24
25
26
27
28
29
30
31
32
33
34
35
36
37
38
39
40
41
42
43
44
45
46
47
48
49
50
51
52
53
54
55
56
57
58
59
60

Introduction

As an important source of information on the big puzzle of hydrogen bonding, medium size ammonia clusters have been attracting increasing attention in the last few years, both from experimentalists and theoreticians. The smallest member of this family, the ammonia dimer, has been subjected to intense experimental scrutiny [1, 2, 3, 4, 5], with a substantial agreement having been reached on its fluxional nature. In fact, theoretical studies have shown that a very low energy barrier separates two identical isomers [6, 7, 8, 9], the latter differing in the H-bond donor and acceptor roles played by the two molecules. As a result of the aforementioned studies on $(\text{NH}_3)_2$, analytical representations for the intermolecular forces between two rigid ammonia molecules have been parameterized, the task having been carried out either by numerically fitting theoretical results [11, 12] or by adjusting analytical models to closely match microwave spectra [10]. We notice that, in these cases, somewhat more emphasis has been placed on providing an adequate description of fundamental microscopic quantities, rather than attempting to accurately reproduce condensed phase data as done previously [13, 14, 15].

As for clusters up to the hexamer, the available experimental data [1, 5, 16, 17] and the related modelling suggested these species possess a structure with little or no electric dipole moment, a finding that was interpreted as possibly indicating ring-like connectivity. However, the presence of a broad IR absorption band [18] in the spectrum of the pentamer was interpreted as an indication of a fluxional nature, possibly making structural assignments more difficult. In this respect, the few theoretical studies available in the literature employing high-level methods [9, 17, 19, 31] all suggested a cyclic structure as the global minimum for the trimer, tetramer and pentamer, with the suggestion for the trimer and tetramer appearing quite robust. In fact, the second lowest lying isomer of $(\text{NH}_3)_3$ and $(\text{NH}_3)_4$ is found, at least, 2 kcal/mol above the ring. However, the extensive investigation on $(\text{NH}_3)_5$ provided in Ref. [9] highlighted the presence of small energy differences (~ 0.2 - 0.4 kcal/mol) between low lying isomers, a finding that makes a definitive assignment for the global minimum quite difficult, and that supports the suggestion of a fluxional nature for the pentamer.

The *ab initio* results in Ref. [9] were also used to evaluate the performance of a few of the available model potential energy surfaces (PES's) for the ammonia-ammonia interaction. Comparing MP2/aug-cc-pVTZ total and relative binding energies with results obtained using analytical models [39, 36], it was found that the available surfaces underestimate binding energies and suggest more compact isomers as global minimum for the pentamer. This is at variance with the results from *ab initio* calculations, which indicated the cyclic species as global minimum. It should be clear that the underestimation of binding energies represents a particular concern for us, given our interest in simulating the process of evaporation/condensation of medium size $(\text{NH}_3)_n$. As a

1
2
3
4
5
6
7
8
9
10
11
12
13
14
15
16
17
18
19
20
21
22
23
24
25
26
27
28
29
30
31
32
33
34
35
36
37
38
39
40
41
42
43
44
45
46
47
48
49
50
51
52
53
54
55
56
57
58
59
60

consequence, the construction of more accurate model potentials seems a necessary step to obtain an improved description for the relative energetics of medium sized $(\text{NH}_3)_n$, an outcome that would manifest itself in a higher accuracy for the predicted dissociation rates. In this respect, we have found the SAPT-based analysis carried out in Ref. [31] on $(\text{NH}_3)_3$ to be extremely useful in pin-pointing the relative importance of several ingredients in obtaining a quantitative description of ammonia–ammonia interactions. In particular, induction forces were highlighted as a key element in providing accurate total interaction energy, induction accounting for at least 70% of the three–body contribution (roughly 10% of the total two–body component). Another important component of the three–body effects was found to be the Heitler-London term; this was however found to be important only for unusual conformations of the trimer, leading us to think that the lack of an explicit treatment of induction forces may be the root–cause of the binding energy underestimation seen for $(\text{NH}_3)_n$ ($n=3-5$). This idea is also supported by the improvement in accuracy provided by the polarizable model built by Dykstra and co–workers [20].

In our view, the above findings stress the necessity for implementing a more accurate model potential for $(\text{NH}_3)_n$. The construction of the latter should be based on *ab initio* energy results and the model should also contain the explicit treatment for the many-body induction component of the interaction forces. Apart from representing an important resource for modeling the structure and energetics of clusters, such a potential may also pave the way toward more accurate statistical and dynamical simulations of condensed phase ammonia.

With this aim in mind, high level *ab initio* calculations have been performed to generate an extensive set of interaction energies for $(\text{NH}_3)_2$. This set of data has been subsequently employed to optimize the parameters of a sensible analytical form for the model potential. In this respect, one should also be concerned with the computational cost of evaluating the model potential, a factor that may hinder its use when it comes to simulate large systems or when employing quantum simulation techniques. The latter are often used to simulate hydrogen bonded species [21, 22, 23], their thermodynamic behaviour being substantially modified by the inclusion of quantum effects.

Employing the new model potential, minimum energy structures for $(\text{NH}_3)_n$ ($n = 6-20$) have been optimized in this work and used in the search for putative global minima and the investigation of the presence of “magic” cluster sizes. The latter are more likely to be detected during molecular beam expansion experiments.

The outline of the paper is as follows. Section II presents the details of the methods employed in this work and the analytical form chosen for the model potential. It also contains a short analysis of the performance of the re–parameterized PES for the ammonia dimer. Section III presents the structural and energetic results for larger clusters, obtained using the model developed in this work. The latter section contains also a comparison

1
2
3 between model PES and electronic structure theory results for $(\text{NH}_3)_n$ ($n = 3 - 5$). Finally, Section IV contains
4 our conclusions and a discussion on possible future work.
5
6
7
8

9 Methods and Results

10 *Ab initio* calculations of monomer properties and dimer interaction energies

11
12 All *ab initio* calculations on the ammonia monomer and dimer were carried out using frozen-core second order
13 Møller-Plesset (MP2) theory and extended basis sets including diffuse functions with the Gaussian 98 and 03
14 suites of codes [24]. The internal geometry of ammonia was kept rigid and identical to the experimental one
15 ($r_{\text{NH}} = 1.021 \text{ \AA}$, $\text{HNH} = 106.67$ degrees) [26]. As for the basis set, it was decided to employ the correlation-
16 consistent family of basis functions optimized by Dunning and co-workers [27], which was previously found to
17 provide a more balanced description of the electrostatic and energetic properties of ammonia clusters than the
18 Pople's family of basis sets [9]. All interaction energies were corrected for the Basis Set Superposition Error
19 (BSSE) using the Counterpoise (CP) procedure proposed by Boys and Bernardi [25].
20
21
22
23
24
25
26
27
28

29 As a test for the performance of our methodological choices, single point calculations on the ammonia
30 monomer were carried out using increasingly larger basis sets to evaluate the rate of convergence of electro-
31 static properties, the latter playing an important role in defining the long range behaviour of the intermolec-
32 ular potential. This is dominated by dipole-dipole and dipole-quadrupole interactions decaying as $1/r^3$ and
33 $1/r^4$, respectively. Table 1 shows the results obtained for the dipole and quadrupole moments using the series
34 MP2/aug-cc-pVxZ ($x = \text{D, T, Q, 5}$); it is clearly seen that both the dipole μ and the quadrupole θ_{zz} have con-
35 verged to at least 99% of their Complete Basis Set (CBS) values at the aug-cc-pVTZ level. When compared
36 with the experimental values (1.47 a.u. and -2.12 a.u., respectively), the *ab initio* results appear to overestimate
37 μ and underestimate θ_{zz} only slightly, indicating the adequacy of the MP2 level to estimate the electrostatic
38 properties of the ammonia molecule. These findings are also in good agreement with the results obtained by
39 Quack and co-workers, who obtained a six dimensional representation for the dipole moment as a function of
40 the molecular geometry [28].
41
42
43
44
45
46
47
48
49
50

51 In our previous work on $(\text{NH}_3)_n$ ($n = 2-5$) [9], it was also established that CP-corrected MP2/aug-cc-pVTZ
52 calculations are capable of estimating interaction energies for the ammonia dimer with high accuracy. Thus,
53 the same level of theory is used here to obtain two dimensional cuts of the PES for $(\text{NH}_3)_2$ as a function of the
54 relative molecular orientation. In choosing the geometries to be explored, we started from the four orientations
55 employed by Hinchliffe *et al.* [12] to generate 1D scans along the N-N distance. The latter was supplemented
56
57
58
59
60

X	μ (a.u.)	θ_{zz}
D	1.5355	-2.12
T	1.5238	-2.09
Q	1.5297	-2.10
5	1.5323	-2.10

Table 1: Values of the dipole (μ) and quadupole (θ_{zz}) moments for the ammonia molecule computed at the MP2/aug-cc-pVxZ level of theory. Experimentally measured values are 1.47 a.u. [29] and -2.12 a.u. [30], respectively.

with a torsional angle to obtain high quality information on the energy barrier for the acceptor–donor exchange, the internal rotation of a single monomer and the global anisotropy of the interaction energy. The coordinates employed in the 2D scans are shown in Figure 1. Apart from the already mentioned N–N distance we employed the angle formed by the two nitrogens and the non donating H in the double donor NH_3 (left panel), a rotation around the C_3 axis of the donating ammonia (center panel), and the angle formed by the C_3 axis of the two molecules. 1D cuts of the 2D MP2 PES along the nitrogen–nitrogen (N–N) distance are shown in Figure 2. From the latter, the strong anisotropy of the $(\text{NH}_3)_2$ model potential is clearly evident. As expected, the “mirror” (D_{3h}) geometry presents a repulsive potential energy curve, due to the relative orientation of the molecular dipoles, whereas the “linear” (σ_v) geometry shows the most favorable interaction due to the hydrogen bond. Interestingly, the “parallel” (C_{3v}) orientation features a long range potential, likely to be due to favorable dipole–dipole and dipole–quadupole interactions.

Parameterization of model potentials

As discussed in the introduction, the comparison between *ab initio* and model potential binding energies for $(\text{NH}_3)_n$ ($n=2-5$) suggested the necessity for more accurate analytical forms. In this respect, we felt that it would be better to select a somewhat more sophisticated form instead of relying simply on nuclear point charges and Lennard-Jones type interactions. Thus, the analytical Model C proposed by Hinchliffe *et al.* [12] was chosen as our starting point, a choice mostly based on the accuracy shown by this form in reproducing Hartree–Fock type calculations with a sensible choice of the various terms composing it. The model [12] assumes the gas phase experimental geometry for the ammonia molecule ($d_{\text{NH}}=1.021 \text{ \AA}$, $\text{HNH}=106.67$ degrees) and approximates the electrostatic interaction using positive point charges Q located on the H atoms, and a negative compensating

charge $-3Q$ located at a distance δ away from the N atom and toward the hydrogens along the C_3 axis of the molecule. The choice of displacing the negative charge from the N atom provides one with an additional parameter, the latter allowing additional flexibility in reproducing the molecular electrostatic properties. In this way, the charge distribution can be set to reproduce exactly the experimental value of the molecular dipole and to provide an accurate value for the quadrupole moment. This is expected to play an important role in defining the anisotropy of the interaction energy, and hence the H-bond structure, in clusters and condensed phases. Following the original implementation by Hinchliffe *at al.*, we chose $Q = 0.462$ a.u. and $\delta = 0.156$ Å.

The exchange–repulsion interaction due to the overlap between the molecular electron densities is represented as a sum of exponential functions $V_{ij}(r_{ij})$ depending on the interatomic distances between *all* atomic pairs (ij)

$$V_{ij}(r_{ij}) = a_{ij} \exp(-b_{ij} \times (r_{ij} - r_{ij}^*)) \quad (1)$$

where r_{ij}^* is an adjustable parameter that defines the onset region of the exponential repulsion. This choice allows one to produce an anisotropic description of exchange–repulsion forces, a feature that is usually lacking in more commonly used potentials such as the one developed by Impey and Klein [13]. Finally, the dispersion component is described using a dumped series of inverse powers in the N–N distance,

$$V_{\text{disp}}(r_{\text{NN}}) = -f(r_{\text{NN}})(d_6/r_{\text{NN}}^6 + d_8/r_{\text{NN}}^8 + d_{10}/r_{\text{NN}}^{10})$$

$$f(r_{\text{NN}}) = 1, r_{\text{NN}} \geq r_*$$

$$f(r_{\text{NN}}) = \exp\left[-\frac{(r_{\text{NN}} - r_*)^2}{r_{\text{NN}}^2}\right], r_{\text{NN}} \leq r_* \quad (2)$$

where the dispersion coefficients have been obtained by means of *ab initio* calculations [32]. In Eq. 2, $r_* = 4.7$ Å and energies are in kcal/mol. With the building of an *ab initio*–based potential, we consider the usage of the dispersion series in Eq. 2 using electronic structure derived dispersion coefficients a more robust approach than relying on simpler r_{NN}^{-6} terms with optimizable parameters. In principle, the latter could be chosen to partially compensate for shortcomings in the choice of other terms in the potential model.

Apart from the discussed terms, the original Model C also included an attractive exponential function meant to improve the description of the H-bond interaction. Such a term was however eliminated from our routines once we noticed that the parameter optimization was making its contribution utterly negligible.

Figure 2 shows 1D cuts of the original Model C [12] together with CP-MP2/aug-cc-pVTZ energies for $(\text{NH}_3)_2$. From this Figure, it is clearly seen that the model potential slightly overbinds (by 0.2 kcal/mol) the ammonia dimer in the linear geometry (i.e. close to the global minimum), that it delays the onset of the repulsive wall in

1
2
3 the parallel and mirror orientations, and that it underestimates the well depth in the “orthogonal” structure.
4
5 We would expect these differences to have a substantial impact on the reorientation dynamics of the ammonia
6
7 molecules.

8
9 Apart from the quantitative differences highlighted in Figure 2, an important limitation of the original
10 Model C is the lack of many-body contributions to the interaction energy, an ingredient that appears essential
11 in building a transferable model. Thus, following the arguments provided in the Introduction, it was decided to
12 supplement the original Model C with an explicit description of induction forces based on the idea of polarizable
13 point dipoles. A suitable method, providing this level of description for the induction component, is represented
14 by the “charge on spring” (COS) model as implemented by van Gunsteren and co-workers [33] for bulk
15 water. This model is reminiscent of the Drude atom, where both polarization and dispersion interactions are
16 represented employing two charges of magnitude q and opposite sign connected by a harmonic spring. Whereas
17 one of these two charges (usually the positive one) is fixed in the molecular framework, the other one is allowed to
18 instantaneously adjust its position in space when subjected to an external uniform electric field (e.g. generated
19 by other molecules) and to the restraining force due to a harmonic spring. Indicating the polarizability of the
20 molecule with α , the external electric field (assumed as uniform) with \mathbf{F} , and the position of the fixed charge
21 with \mathbf{r}_0 , the equilibrium position of the moving charge \mathbf{r}_m is given by [33]
22
23
24
25
26
27
28
29
30
31
32

$$\mathbf{r}_m = \mathbf{r}_0 - \alpha\mathbf{F}/q \quad (3)$$

33
34
35
36
37 Guided by MP2/aug-cc-pVTZ calculations, which give $\alpha_{xx} = 13.634$, $\alpha_{yy} = 13.630$, and $\alpha_{zz} = 15.299$ in a.u.,
38 an isotropic polarizability α is assumed in Eq. 3 for ammonia. We expect this assumption to be sufficiently
39 accurate for small symmetric molecules in absence of charged species [34].
40
41
42

43 In a molecular aggregate, Eq. 3 should be iterated until convergence to account for the changes in magnitude
44 and direction of the external electric field experienced by a molecule as a consequence of the polarized charge
45 distribution. This is in order to provide a self-consistent description of the induction process and the magnitude
46 of the final molecular dipoles needed to estimate the induction energy. However, it has been shown recently
47 that more than 95% of the point dipole induction energy in water aggregates is already recovered after the first
48 iteration of Eq. 3 [35]. So, we also tested a non-iterative (single-step) version of the COM model, which has
49 the advantage of reducing the total cost of the potential and of providing one with an energy surface that is
50 intrinsically free of discontinuities. In our implementation of the COS model, the fixed charge was placed on the
51 N atom; it was also decided to employ charges of magnitude $q = 16$ a.u., twice as large as the one used by van
52 Gunsteren and co-workers. The effect of a larger q is to reduce the magnitude of the free charge displacement
53
54
55
56
57
58
59
60

for a given external field, an outcome that helps in fulfilling the hypothesis of point-like dipoles underlying the results presented in Ref. [35]. As an additional motivation for using a larger q in the COS model, a quantitative discussion on the effect that substituting a point dipole with the COS one has on the total accuracy of the induction interaction is provided in Appendix A.

With above choices for the fictitious charges, the location of the polarizable centre in ammonia, and the MP2-CBS value for the spherically averaged molecular polarizability ($\alpha_{\text{MP2}} = 2.103 \text{ \AA}^3$), the non-iterative procedure was consistently found to provide us with more than 95% of the self-consistent estimate of the induction energy in ammonia clusters. When employing the single-step COS approach, the latter quantity is estimated using [35]

$$V_{ind} = \sum_i -\frac{1}{2} \mu_i^{(0)} \cdot E_i^{(0)} - \frac{1}{2} \mu_i^{(0)} \cdot E_i^{(1)} \quad (4)$$

In Eq. 4, $E_i^{(0)}$ is the initial external field experienced by the i -th molecule resulting from the fixed point charges of other molecules, $\mu_i^{(0)}$ is the dipole induced in the i -th molecule as obtained substituting $E_i^{(0)}$ into Eq. 3, and $E_i^{(1)}$ is the field experienced by the same molecule due to the induced component of the dipole in other molecules. As a consequence of this good performance by the single-step COS model, we feel confident in using it as an alternative to the more standard self-consistent approach to induction energy. Noteworthy, the usage of a single iteration makes the induction model chosen in this work to be independent of the order in which molecules are treated; this is easily understood remembering that the polarizing field is generated by the distribution of the fixed atomic charges.

Preliminary Monte Carlo simulations have revealed that with decreasing distances between atoms of different molecules (less than one bohr), V_{ind} , at first repulsive, eventually becomes large and negative, causing walkers to remain trapped in unphysical configurations. The situation persists even when a large number of iterations is performed. Therefore, a multiplicative switching function is used to turn off V_{ind} smoothly,

$$S(r) = \frac{1}{2} \{1 + \tanh [10(r - 1)]\} \quad (5)$$

where r in Eq. (5) is the distance between any atom in molecule i and the nitrogen atom in molecule j .

The free parameters of the analytical form (i.e. a_{ij} , b_{ij} , $1r_{ij}^*$, r_* , but not d_6 , d_8 , and d_{10}) were optimized minimizing the least square error between the *ab initio* and model potential interaction energies over the set of configurations explored by our scans. In order to improve the description of regions close to the equilibrium and relevant to the low energy dynamics, geometries with negative interaction energy were given fivefold larger weights than any others in order to favor a more accurate fit. Several sets of initial values for the parameters were used as a way of exploring for the presence of multiple minima in the cost function, the set providing the

lowest error being shown in Table 2 under the heading Model C(pol, Q^{frozen}). In spite of the risk of spoiling the description of the long range interaction, the charge magnitude Q was subsequently included in the set of optimizable parameters, the minimization of the least square error resulting in the set shown in Table 2 under the heading Model C(pol, Q^{opt}). As apparent from Table 2, the parameters describing the H-H interaction (namely a_{HH} and b_{HH}) and r_* were kept identical to the ones of the original Model C [12], the reason for this choice being that their optimization did not bring any substantial improvement in the quality of the model interaction. We relate this fact to a very flat behaviour of the cost function along these variables.

Figure 3 shows 2D surfaces representing the signed difference between the *ab initio* interaction energies and the three model potentials described by the parameters in Table 2. The coordinates used in the plots are the N-N distance and the angle formed between the N-N direction and the C_3 axis of one of the ammonia molecules when the “mirror” geometry (see Fig. 2) – with one of the molecules rotated by 60 degrees around the C_3 axis to form a staggered conformation – is chosen as reference structure ($\theta = 0$). So, the region around $\theta \sim 0$ represents the “N to N” approach of the two molecules, the one with $\theta \sim 80$ represents a linear H-bond configuration, and when $\theta \sim 180$ the two molecules are approaching each other in the “parallel” geometry.

Comparing the plots suggests that a substantial improvement in accuracy is obtained for Model C(pol, Q^{frozen}) and Model C(pol, Q^{opt}) as a consequence of the optimization. In particular, the error along the “mirror” and “parallel” approaches is reduced by a factor of ~ 2 with respect to the original potential. At a finer level of detail, we notice that optimizing Q slightly reduced the well depth in the “linear” configuration, inducing also a substantial improvement in the description of the “mirror” orientation when compared to Model C(pol, Q^{frozen}). The improved description of this geometry may have important consequences in the description of the ammonia “tumbling” dynamics in the liquid phase and in the relative energetics of isomeric clusters, especially when ammonia molecules act as double-acceptors of H-bonds. We also point out that the accurate long range behaviour for the intermolecular interaction provided by the initial choice of $Q = 0.462$ a.u. appears to be conserved even after the optimization of Q , the point-charge magnitude, with both Model C(pol, Q^{frozen}) and Model C(pol, Q^{opt}) presenting only small deviations (at most 0.2 kcal/mol) from the MP2 values.

Conclusions similar to the ones just presented are obtained analyzing the difference between the optimized models and the other two sets of *ab initio* data used as training sets; in both cases, Model C(pol, Q^{opt}) appears to perform slightly better than Model C(pol, Q^{frozen}). We would therefore suggest the former to be used in describing intermolecular interactions between ammonia molecules.

To test for the quality of Model C(pol, Q^{opt}) in reproducing the structural details of the rigid ammonia dimer, the geometry of the latter was optimized using our calibrated PES. Geometrical results are provided in

Parameters	Model C [12]	Model C(pol, Q^{opt})	Model C(pol, Q^{frozen})
a_{NN}	13615	9162.98329	6903.06545
b_{NN}	-2.7	2.63500285	2.35033248
r_{NN}^*	0.0	0.0	0.0
a_{NH}	0.4	0.427713623	0.247394716
b_{NH}	2.3	3.60109836	3.66458152
r_{NH}^*	2.5	2.606558	2.73514533
a_{HH}	700	700.0	700.0
b_{HH}	3.7	3.7	3.7
r_{HH}^*	0.0	0.0	0.0
r_*	4.7	4.7	4.7
Q	0.462	0.526420468	0.462
δ	0.156	0.156	0.156
d_6	1230	1230	1230
d_8	6500	6500	6500
d_{10}	42100	42100	42100

Table 2: Optimized parameters for the two model potentials Model C(pol, Q^{opt}) and Model C(pol, Q^{frozen}). Also shown are the parameters for the original analytical form Model C [12], where the analytical form $V_{ij}(r_{ij}) = a_{ij} [\exp(-b_{ij} \times (r_{ij} - r_{ij}^*)) - 1]^2 - a_{ij}$ was used to describe the interaction between N and H atoms in different molecules. Several significant figures are reported for the optimized parameters to guarantee an accurate reproduction of the new model potentials. Units are: kcal/mol for a_{ij} ; \AA^{-1} for b_{ij} ; \AA for r_{ij}^* , δ and r_* ; a.u. for Q . The units of the dispersion parameters d_6 , d_8 , and d_{10} are respectively kcal/(mol \AA^6), kcal/(mol \AA^8), and kcal/(mol \AA^{10}).

Figure 4; from this, one could notice the good agreement with the CP-MP2/aug-cc-pVTZ level of theory, the analytical form slightly overestimating the N–N distance and the NHN angle of the hydrogen bond. As for the binding energy, Model C(pol, Q^{opt}) was found to slightly underestimate the *ab initio* value (~ 0.162 kcal/mol), correcting the tendency of the original Model C that was suggesting a more strongly bound dimer.

Structure and energetics of $(\text{NH}_3)_n$ ($n = 3 - 20$)

Minimum energy structures for larger ammonia clusters were optimized employing Model C(pol, Q^{opt}) as PES. The geometry optimization was carried out in a manner similar to the one suggested by Beu and Buck [36], i.e. starting from randomly positioned and oriented ammonia molecules inside a cube of side 15–20 Å. For every $(\text{NH}_3)_n$ ($n = 3 - 20$), several thousand structures were optimized by minimizing the total energy with the Powell method [37], producing a database of local minima for each n . Putative global minima were extracted and their structure is shown in Figures 5 and 6 (atomic positions and energies for the clusters shown in Figs. 5 and 6 are available from the Authors upon request).

In the following sections, the structural and energetics results obtained from this procedure are presented. We begin with discussing the performance of Model C(pol, Q^{opt}) in reproducing the *ab initio* data available in the literature for $n = 3 - 5$ [9]. The results for the larger clusters are successively compared with other studies carried out employing different model interactions.

$(\text{NH}_3)_n$ ($n = 3 - 5$)

The top row of Figure 5 shows the three putative global minima for $(\text{NH}_3)_3$, $(\text{NH}_3)_4$, and $(\text{NH}_3)_5$. Their total binding energy is given in Table 3. Both the trimer and tetramer global minima present a cyclic structure which facilitate the formation of strong hydrogen bonds, a finding that agrees well with *ab initio* results [9]. Comparing CP-MP2/aug-cc-pVTZ and model potential energies for $n = 3$ and 4, one notices that Model C(pol, Q^{opt}) slightly underestimates the cluster total binding energy. In spite of this, Model C(pol, Q^{opt}) represents a substantial improvement with respect to previously available model potentials, which were found to underestimate this same quantity substantially more than the present analytical surface, particularly in the case of the tetramer (see Table 3 and Ref. [9] for a detailed comparison). Interestingly, Model C(pol, Q^{opt}) appears to provide performance similar to the CP-MP2/aug-cc-pVDZ level of theory in predicting the total binding energy for the trimer and tetramer. It is perhaps worth noting that the search for the tetramer global minimum produced an isomer composed by a three-member ring with an external ammonia molecule (the “tail” isomer first presented in Ref. [9]), suggesting the likelihood of generating this species during sequential pick-up

n	Model C(pol, Q^{opt})	CP-MP2/aug-cc-pVTZ	CP-MP2/aug-cc-pVDZ	Beu and Buck [36]	Model C
3	9.055	10.067	9.326	8.258	9.073
4	14.908	15.515	14.427	12.628	13.433
5 (Cyclic)	19.4464	19.358	18.334		
5 (Compact)	18.3424	19.203	18.127		
5 (BB1)	18.2646	19.315	18.177	16.720	
5 (Pyramid)	18.1238	19.263	18.181		
5 (Butterfly)	17.4385	18.45	17.21		

Table 3: Total binding energy (kcal/mol) for the putative global minima of $(\text{NH}_3)_n$ ($n = 3 - 5$) computed using Model C(pol, Q^{opt}) and CP-MP2/aug-cc-pVTZ [9]. Also shown are the binding energy for the four lowest lying isomers of $(\text{NH}_3)_5$.

of ammonia molecules in superfluid He droplets. This event may be facilitated by the fact that, during the pick up process, the cyclic trimer might form before the fourth ammonia molecule is added to the droplet. However, recent IR spectra of small $(\text{NH}_3)_n$ in He droplets [17] appeared to provide no support for the presence of the "tail" (or 3+1 [17]) isomer, a finding that might suggest the possibility of the fourth ammonia molecule entering the ring as a consequence of the addition dynamics. This event would clearly require the partial opening of the ring, a process that appears to take place during the sequential pick up of water molecules in He droplets [38].

Also shown in Table 3, there is the binding energy for the cyclic trimer and tetramer computed using the original Model C. Whereas the energy of the trimer computed using Model C agrees well with the one obtained with Model C(pol, Q^{opt}), the situation is different for the tetramer, for which Model C appears to substantially underestimate the binding. Perhaps even more important it is the fact that Model C predicts a more compact tetrahedral isomer as the lowest energy species instead than the ring as done by the *ab initio* calculations and by Model C(pol, Q^{opt}).

As far as the pentamer is concerned, previous *ab initio* calculations have provided evidence for a compressed energy landscape: five isomers were found to lie within 2 kcal/mol from the putative global minimum, with four of those isomers lying within 0.3 kcal/mol from the lowest one. Thus, $(\text{NH}_3)_5$ represents a challenging test for the new model potential. The energy results for the five lowest energy pentamers obtained using Model C(pol, Q^{opt}) are reported in Table , together with the corresponding *ab initio* energies computed after an optimization at the MP2/aug-cc-pVDZ level. We notice that a new isomer ("butterfly") was produced during the global minimum

1
2
3
4 search that was not previously studied in Ref. [9], its structure being shown in Figure 7. At first glance, we
5
6 found it pleasing that Model C(pol, Q^{opt}) appears capable of predicting the correct lowest energy isomer with
7
8 a difference between *ab initio* and model results of only 0.1 kcal/mol. This represents a substantially better
9
10 agreement than in the case of the trimer and tetramer. Bearing in mind that Model C(pol, Q^{opt}) underestimates
11
12 the binding energy of the dimer by 0.162 kcal/mol and that this effect is likely to be additive, we suspect the
13
14 improvement in performance to be mostly due to the many-body induction term in our energy expression.

15
16 From Table 3, we notice that the five isomers with higher energy are predicted to lie at least 1.0 kcal/mol
17
18 above the cyclic species, at slight variance with the MP2 calculations. A possible explanation for this finding
19
20 is provided by the 2D cuts shown in Fig. 3, from which is apparent that Model C(pol, Q^{opt}) lies above the
21
22 MP2 surface for NHN angles differing from $\sim 80^\circ$, i.e. the linear H-bond geometry. Thus, the model appears
23
24 to introduce some energy penalty for all isomers but the cyclic one, whose hydrogen bonds deviate the least
25
26 amount from linearity compared to other species. This artificial increase in the interaction energy may also
27
28 explain the fact that Model C(pol, Q^{opt}) produces a cyclic pentamer that is flatter than the one obtained using
29
30 CP-corrected MP2. Nevertheless, these five local minima are predicted to lie very close to each other, in
31
32 agreement with the MP2 calculations [9]. In retrospect, it would seem sensible to accept that reproducing
33
34 accurately the compressed energy ranking provided by the *ab initio* results would have been difficult for any
35
36 model potential. What one could have hoped for, instead, is to have obtained a consistent performance in
37
38 providing reasonable energies for the lowest isomers, something that Model C(pol, Q^{opt}) seems to be capable of.
39
40 In this respect, the new model appears as a substantial improvement when compared to the original Model C,
41
42 the latter predicting a novel more compact isomer as lowest energy species for $(\text{NH}_3)_5$. In practice, we failed to
43
44 recognise the presence of the cyclic isomer in a set of 2000 structure optimized using Model C, and even when
45
46 starting from a pre-optimized cyclic geometry, Model C produced a previously unobtained tetrahedral species.
47
48 Out of the 2000 new pentamer structures obtained with Model C, we managed to recognize only the previously
49
50 discussed BB2 isomer [9], which was not however obtained when using Model C(pol, Q^{opt}). Indeed, we suspect
51
52 the root-cause of these findings to be related to the presence of a Morse-like interaction between the nitrogen
53
54 and the hydrogens of two different molecules that was introduced to improve the description of the hydrogen
55
56 bond interaction. As mentioned before, our parameter optimization invariably led to a negligible contribution
57
58 from this part of the model, which was therefore eliminated.

59
60 Apart from the species listed in Table 3, several other isomers were located during the structural search,
invariably presenting a reduced number of H-bonds than the 5 lowest minima. At this stage, we consider
worth mentioning the optimization of a linear species (BE=14.88 kcal/mol) and of an isomer composed by a

three-member ring connected to a two-member chain ($BE=15.31$ kcal/mol). The appearance of the latter is of particular interest, since it might be possible to form it inside superfluid He droplets. Thus, we tested the stability of this isomer by performing MP2/aug-cc-pVDZ optimizations, which indicated the propensity of this species to isomerize into one of the compact species previously investigated in Ref. [9]. This effectively leaves the four-member ring with a single ammonia tail found in Ref. [9] as the only stable non-compact structure obtained in our search for stationary points of $(\text{NH}_3)_5$.

$(\text{NH}_3)_n$ ($n = 6 - 20$)

Figures 5 and 6 present the structure of the putative global minimum for $n = 6 - 20$, while the binding energy of three lowest lying isomers for each $(\text{NH}_3)_n$ is shown in Table 4. A more comprehensive picture of the relative energetics for every cluster size is given in Figure 8. Here, the relative energy of the first 200 local minima with respect to lowest isomer is shown. Binding energies obtained using different model potentials [36, 39] are also shown in Table 4 for comparison. From these, one can notice that Model C(pol, Q^{opt}) consistently predicts larger binding energies than previous investigations, an outcome possibly due to the many-body induction term.

Directly related to the relative stability of different cluster sizes, another interesting energetic quantity is represented by the molecular evaporation energy. This is defined as the energy required to adiabatically detach an ammonia molecule from a given cluster ($E_{vap}(N) = E_n - E_{n-1}$), and its behaviour is shown in Figure 9 as a function of n for Model C(pol, Q^{opt}) and for the binding energy results obtained by Beu and Buck [36] employing the Impey and Klein potential [13]. From Fig. 9, one notices that Model C(pol, Q^{opt}) presents a rougher behaviour for E_{vap} than the one obtained using the simpler pair-wise model employed in Ref. [36]. Of particular interest in the plot is the large value of E_{vap} predicted by Model C(pol, Q^{opt}) for $n=8, 10, 12, 15$ and 20 , a finding that seems to indicate the possible presence of magic numbers. Taken as a whole, the different behaviours shown by $E_{vap}(n)$ as a function of the model potential stress the importance of the induction term in defining the relative stability of ammonia clusters with different sizes.

As far as the geometries of the lowest minima are concerned, a quick glance at Figs. 5 and 6 suggest that these may be partitioned in two classes using the “regularity” of their structure as a criterion. More specifically, we notice that the structure of the lowest $(\text{NH}_3)_6$, $(\text{NH}_3)_8$, $(\text{NH}_3)_{10}$, and $(\text{NH}_3)_{12}$ are based either on simple geometrical shapes or on regular polyhedra, a finding that provides additional support for the possible role of $n=8, 10$, and 12 as magic numbers. In the case of the hexamer, we also notice that the lowest minimum for this cluster presents a flat structure (“book”) which can be described as two fused tetramers (or two fused squares); in this, one notices the appearance of both a double donor and double acceptor molecules. Alternatively, the

n	I	II	III	Beu and Buck [36]	Greer <i>et al.</i> [39]
6	24.29	24.03	23.77	22.70	22.73
7	30.142	29.993	29.587	28.23	28.53
8	37.311	36.609	35.943	34.12	
9	42.042	41.993	41.892	39.48	
10	48.786	48.485	48.2381	45.59	
11	55.211	54.726	54.668	51.22	
12	62.231	62.180	60.978	58.41	
13	67.881	67.323	67.112	62.97	
14	73.363	73.330	73.2596	69.06	
15	80.924	80.228	80.055	74.92	
16	87.045	86.181	86.134	81.51	
17	91.040	90.333	89.968	87.46	
18	97.958	97.666	97.213	93.73	
19	101.634	100.700	100.409		
20	111.536	111.009	110.023		

Table 4: Total binding energy (kcal/mol) for the three lowest energy isomers of $(\text{NH}_3)_n$ ($n = 6 - 20$) obtained using Model C(pol, Q^{opt}). Also shown are the binding energies of the lowest energy isomers found by Beu and Buck (Ref. [36]) and by Greer *et al.* (Ref. [39]).

1
2
3 relative disposition of the N atoms can be described as deriving from the “chair” structure typical of the lowest
4 conformer of cyclohexane. This structure is at variance with the results of previous investigations employing
5 non-polarizable models [36, 39], which suggested a more compact 3D geometry as global minimum. A 3D
6 structure is however obtained for the second lowest isomer (Fig. 7), the latter lying only 0.26 kcal/mol above
7 the putative global minimum. Given this small energy difference between the two species, it may prove necessary
8 to employ electronic structure calculations to conclusively assign the global minimum structure.
9
10

11
12
13
14 As for $(\text{NH}_3)_8$, we found both the global minimum and second lowest isomer to present a structure based
15 on a distorted cubic shape that are built starting from two different isomers of the tetramer. In particular, the
16 tetramers in the lowest isomer are characterized by an alternate disposition of the free H atoms with respect
17 to the ring plane (UDUD, where U and D indicate the direction of the free NH bond for an ammonia molecule
18 perpendicular to the plane as pointing up or down, respectively). In contrast, the second one has the two
19 tetrameric moieties showing a UUDD orientation of the free NH bonds. It is also interesting to notice that the
20 lowest isomer found has a higher symmetry (D_{2d}) than the second one, the latter presenting only a binary axis.
21 This difference in the relative arrangement of hydrogen bonds (see Fig. 7 for the structure of the second isomer)
22 is reflected in an energy gap of 0.702 kcal/mol between the two species. Another substantial energy gap (0.666
23 kcal/mol) separates the second from the third isomer of $(\text{NH}_3)_8$ (see Fig. 7 for a global view of the energetics),
24 a finding suggesting in our view the possibility that the low temperature thermodynamics of the octamer is
25 likely to be dominated by its global minimum, and that it should be expected to present signatures for a phase
26 transitions in the specific heat as found in the case of $(\text{H}_2\text{O})_8$ [40].
27
28
29
30
31
32
33
34
35
36
37

38 A somewhat similar situation is also found for the decamer, with sizable energy gaps being found between
39 the lowest three or four isomers. It is noteworthy that the lowest energy isomer for $(\text{H}_2\text{O})_{10}$ can be seen as built
40 from the global minimum for the octamer adding the two additional molecules on the same cube face. Being
41 connected between themselves, these two molecules also accept and donate hydrogen bonds with molecules
42 on the face, forming two three-member rings and leaving a binary axis as the only symmetry element for the
43 structure.
44
45
46
47
48

49 A more interesting case in terms of the competition between different structures for the title of global
50 minimum is provided by $(\text{NH}_3)_{12}$, for which an icosahedral geometry, separated from the second lowest isomer
51 by 1.8 kcal/mol, was predicted [36]. At variance with this result, our optimization generated two species
52 extremely close in energy (0.051 kcal/mol) presenting completely different geometries. Whereas the second one
53 can be described as composed by two cubes fused on a face (Fig. 7), the lowest of the two isomers has the
54 same icosahedral structure and evaporation energy found in Ref. [36]. Apparently, the explicit description of
55
56
57
58
59
60

1
2
3 the electronic induction present in our model does not play an important role in the relative energetics for the
4 global minimum of $(\text{NH}_3)_{12}$, a finding that might be due to the high symmetry of this species. Interestingly,
5 the geometry of the second lowest isomer is similar to the global minimum proposed for $(\text{H}_2\text{O})_{12}$ (see Ref. [41]
6 for an analysis based on H-bond topology, and references cited in Ref. [42] for a discussion). There is, however,
7 an important difference between the fused structure for $(\text{NH}_3)_{12}$ and $(\text{H}_2\text{O})_{12}$, namely the fact that the number
8 of isomers differing only due to the relative disposition of H-bonds is lower in the case of the former than for
9 the latter. A thorough analysis of this fact and of its consequence is, however, outside the scope of this work
10 and it is therefore postponed. Also noteworthy is the large gap (1.202 kcal/mol) present between the two lowest
11 isomers and the third one; the latter suggests that signatures for a structural transformation may be found in
12 the specific heat of this cluster. As a final comment on the dodecamer, we stress the necessity for high level *ab*
13 *initio* calculations to provide an accurate prediction of the relative energetics for the two low lying species.
14
15
16
17
18
19
20
21
22
23

24 Finally, we turn to comment on the clusters presenting a less regular disposition of the N atoms. In this
25 case, we notice that species containing an even number of ammonia molecules seem to present a more spherical
26 structure than aggregates composed by an odd number of NH_3 . In the case of the latter, the lack of sphericity
27 (or better of an inversion centre) opens the possibility of a non-zero dipole moment of the cluster. Bearing
28 in mind the substantial energy gap between low lying isomers shown in Fig. 8 and the usually low internal
29 temperature of the clusters, it seems likely that odd number clusters may present a non-zero dipole moment,
30 therefore allowing their separation from even n species by means of a non-uniform electric field. The only
31 exception to this simple rule appears to be $(\text{NH}_3)_{13}$, which possesses a shape closely related to the dodecamer.
32 In fact, we noticed that the global minimum of $(\text{NH}_3)_{13}$ may be obtained by “squashing” the thirteenth molecule
33 onto one edge of $(\text{NH}_3)_{12}$, a finding that is, once again, at variance with what was previously found with a pair-
34 wise model [36]. In the latter case, the structure of the lowest energy isomer for $n=13$ was derived from the
35 dodecamer one by having the thirteenth ammonia molecule accepting a hydrogen bond from one of the NH_3
36 forming the icosahedron.
37
38
39
40
41
42
43
44
45
46
47
48

49 Conclusions

50
51 In this work, the implementation of a new model describing the interaction between ammonia molecules has
52 been discussed, its analytical form being partially based on a previous suggestion by Hinchliffe *et al.* [12].
53 Additionally, the model presents an explicit many-body description of the induction energy at the level of dipole
54 polarizability, a feature that was not previously available in other semiempirical forms. The term describing the
55 effect of induction has been implemented using the non-iterative “charge on spring” scheme proposed by van
56
57
58
59
60

1
2
3
4
5
6
7
8
9
10
11
12
13
Gunsteren and co-workers [33], assuming an isotropic polarizability for NH_3 . The free parameters of the new model have been obtained minimizing the least square error with a set of CP-MP2/aug-cc-pVTZ interaction energies computed over configurations relevant for the low energy dynamics of the ammonia dimer. As a consequence of this optimization, two improved models have been obtained, both describing the interaction between two ammonia molecules with a higher accuracy than the original parameterization of the analytical form.

14
15
16
17
18
19
20
21
22
23
24
25
26
27
28
Employing the most accurate model (i.e. Model C(pol, Q^{opt})), a search for the structure of the global minimum of $(\text{NH}_3)_n$ ($n=3-20$) was carried out. Energy results for $n=3-5$ were used to test the transferability of our model PES against *ab initio* data, suggesting that a substantial improvement in accuracy has been obtained with this new potential. A new low energy isomer was also found for $(\text{NH}_3)_5$, its energy and structural details having been tested using electronic structure calculations. As for larger clusters, our model potential predicts larger binding energies than suggested by previous investigations employing pairwise potentials. Our data also indicate a rougher behaviour of the evaporation energy as a function of the number of ammonia molecules in the cluster, a feature suggesting the presence of magic numbers for $n = 8, 10, 12, 15$ and 20 .

29
30
31
32
33
34
35
36
37
38
39
40
41
42
43
44
We expect the improved performance provided by Model C(pol, Q^{opt}) with respect to previously employed interaction potentials to pave the way for more accurate simulations of ammonia aggregates (both clusters and bulk liquid). Here, we briefly mention the possibility of studying the effects of quantum nuclear motion on the thermal properties of small and medium clusters. In this respect, previous studies on hydrogen bonded clusters have highlighted the importance of correctly including quantum effects for an accurate prediction of their relative stability [21] and of their thermodynamic behaviour [23]. Of particular interest to us, there is also the prediction of cluster dissociation rate as a function of n at the level of Transition State Theory.

45 46 47 48 49 50 51 52 53 54 55 56 57 58 59 60 **Acknowledgments**

The authors acknowledge Samuel L. Stone for a careful read of the manuscript. MM acknowledges an EP-SRC Advanced Research Fellowship (GR/R77803/01). E. C. acknowledges support from the National Science Foundation (Grant number CHE0554922), and the donors of the Petroleum Research Fund, (Grant number 40946-B6)

Appendix A

In this Appendix, we provide the reader with a brief discussion on the accuracy of substituting the point dipole approach with the COS model when computing the value of the electric field generated by an induced dipole. Indicating with \mathbf{x} the displacement of the negative charge ($-|q|$) in the COS model when subjected to an uniform external field, one can write the contribution to the field due to the new charge distribution at a point \mathbf{y} in space as

$$\mathbf{F}_{ind}(\mathbf{y}) = \frac{|q|(\mathbf{r} - \mathbf{y})}{|\mathbf{r} - \mathbf{y}|^3} - \frac{|q|(\mathbf{r} + \mathbf{x} - \mathbf{y})}{|\mathbf{r} + \mathbf{x} - \mathbf{y}|^3} \quad (6)$$

Here, \mathbf{r} is the position of the positive compensating charge fixed in the molecular framework. Expanding $\mathbf{F}_{ind}(\mathbf{y})$ in Taylor series with respect to \mathbf{x} , one can show that the difference between the induced field given by Eq. 6 and by the point dipole formulae

$$F_{ind}^r(\mathbf{y}) = \frac{\mu_{ind} \cos(\theta)}{r^3} \quad (7)$$

$$F_{ind}^\theta(\mathbf{y}) = \frac{\mu_{ind} \sin(\theta)}{r^3} \quad (8)$$

is second order in $|\mathbf{x}|/r$, or that, using Eq. 3, it is inversely proportional to $|q|^2$. In Eqs. 7 and 8, $\mu_{ind} = |q\mathbf{x}|$, r is the distance between the point dipole and the position \mathbf{y} , θ is the angle between the direction of the dipole and the line connecting it to \mathbf{y} , while F_{ind}^r and F_{ind}^θ are the components of the induced field parallel and perpendicular to the same line. In turn, this fact indicates that one could alternatively use Eq. 6 or Eqs. 7 and 8 to evaluate the induced field $\mathbf{F}_{ind}(\mathbf{y})$ or the induction energy (Eq. 4) as long as the magnitude of the negative charge displacement is kept small with respect to the distance r . Numerical estimates for the charge separation in the presence of an external field similar to what is expected in ammonia clusters suggests that $|q| = 16$ a.u. is a reasonable magnitude for the COS fluctuating charge.

References

- [1] Odutola, J. A.; Dyke, T. R.; Howard, B. J.; Muentner, J. S., *J. Chem. Phys.*, **1979**, *70*, 4884.
- [2] Nelson, D. D. Jr.; Fraser, G. T.; Klemperer, W., *J. Chem. Phys.*, **1985**, *83*, 6201.
- [3] Nelson, D. D. Jr.; Klemperer, W.; Fraser, G. T.; Lovas, F. J.; Suenram, R. D., *J. Chem. Phys.*, **1987**, *87*, 6364.
- [4] Süzer, S.; Andrews, L. *J. Chem. Phys.*, **1987**, *87*, 5131.
- [5] Snels, M.; Fantoni, R.; Sanders, R.; Meerts, W. L., *Chem. Phys.*, **1987**, *115*, 79.
- [6] Cybulski, S. M., *Chem. Phys. Lett.*, **1994**, *228*, 451.
- [7] Lee, J. S.; Park, S. Y., *J. Chem. Phys.*, **2000**, *112*, 230.
- [8] Stålring, J.; Schütz, M.; Lindh, R. Karlstrom, G.; Widmark, P-O., *Mol. Phys.*, **2002**, *100*, 3389.
- [9] P. E. Janeiro-Barral and M. Mella, *J. Phys. Chem. A* **110**, 11244 (2006).
- [10] Olthof, E. H. T.; van der Avoird, A.; Wormer, P. E. S., *J. Chem. Phys.*, **1994**, *101*, 8430.
- [11] Sagarik, K. P.; Ahlrichs, R.; Brode, S., *Mol. Phys.*, **1986**, *57*, 1247.
- [12] A. Hinchliffe, D. G. Bounds, M. L. Klein, I. R. McDonald and R. Righini, *J. Chem. Phys.* **74**, 1211 (1981).
- [13] R. W. Impey and M. L. Klein, *Chem. Phys. Lett.* **104**, 579 (1984).
- [14] I. R. McDonald and M. L. Klein, *J. Chem. Phys.*, **64**, 4790 (1976).
- [15] M. L. Klein, I. R. McDonald, and M. Righini, *J. Chem. Phys.*, **71**, 3673 (1979).
- [16] Huisken, F.; Pertsch, T. *Chem. Phys.*, **1988**, *126*, 213.
- [17] Slipchenko, M. N.; Sartakov, B. G.; Vilesov, A. F.; Xantheas, S. S., *J. Phys. Chem. A*, **2007**, *111*, 7460.
- [18] Heijmen, B.; Bizzarri, A.; Stolte, S.; Reuss, J., *Chem. Phys.*, **1988**, *126*, 201.
- [19] Kulkarni, S. A.; Pathak, R. K., *Chem. Phys. Lett.*, **2001**, *336*, 278.
- [20] Dykstra, C. E.; Andrews, L., *J. Chem. Phys.*, **1990**, *92*, 6043.
- [21] J. K. Gregory and D. C. Clary, *J. Phys. Chem.* **100**, 18014 (1996).

- 1
2
3
4 [22] M. Mella and D. C. Clary, *J. Chem. Phys.* **119**, 10048 (2003).
5
6 [23] M. W. Aviles and P. T. Gray and E. Curotto, *J. Chem. Phys.* **124**, 174305 (2006).
7
8 [24] Gaussian 98, Revision A.11.1, M. J. Frisch, G. W. Trucks, H. B. Schlegel, G. E. Scuseria, M. A. Robb,
9 J. R. Cheeseman, V. G. Zakrzewski, J. A. Montgomery, Jr., R. E. Stratmann, J. C. Burant, S. Dapprich,
10 J. M. Millam, A. D. Daniels, K. N. Kudin, M. C. Strain, O. Farkas, J. Tomasi, V. Barone, M. Cossi, R.
11 Cammi, B. Mennucci, C. Pomelli, C. Adamo, S. Clifford, J. Ochterski, G. A. Petersson, P. Y. Ayala, Q.
12 Cui, K. Morokuma, P. Salvador, J. J. Dannenberg, D. K. Malick, A. D. Rabuck, K. Raghavachari, J. B.
13 Foresman, J. Cioslowski, J. V. Ortiz, A. G. Baboul, B. B. Stefanov, G. Liu, A. Liashenko, P. Piskorz, I.
14 Komaromi, R. Gomperts, R. L. Martin, D. J. Fox, T. Keith, M. A. Al-Laham, C. Y. Peng, A. Nanayakkara,
15 M. Challacombe, P. M. W. Gill, B. Johnson, W. Chen, M. W. Wong, J. L. Andres, C. Gonzalez, M. Head-
16 Gordon, E. S. Replogle, and J. A. Pople, Gaussian, Inc., Pittsburgh PA, 2001.
17
18 [25] Boys and M. Bernardi, *Mol. Phys.* **19**, 553 (1970).
19
20 [26] W. S. Benedict, N. Gailar, and E. K. Plyler, *Can. J. Phys.* **35**, 1235 (1957).
21
22 [27] D. E. Woon and T. H. Dunning Jr., *J. Chem. Phys.* **98**, 1358 (1993).
23
24 [28] R. Marquardt, M. Quack, I. Thanopoulos, and D. Luckhaus, *J. Chem. Phys.* **119**, 10724 (2003).
25
26 [29] D. K. Coles, W. E. Good, J. K. Bragg, and A. H. Sharbaugh, *Phys. Rev.*, **82**, 877 (1951).
27
28 [30] S. G. Kukolich, *Chem. Phys. Lett.* **5**, 401 (1970).
29
30 [31] Szczyński, M. M.; Kendal, R. A.; Chalasiński, G., *J. Chem. Phys.*, **1991**, 95, 5169.
31
32 [32] iG. D. Zeiss and W. J. Meath, *Mol. Phys.* **33**, 1155 (1997).
33
34 [33] H. Yu, T. Hansson, and W. F. van Gunsteren, *J. Chem. Phys.*, **118**, 221 (2003).
35
36 [34] G. Duquette, T. H. Ellis, G. Scoles, R. O. Watts, and M. L. Klein, *J. Chem. Phys.*, **68**, 2544 (1978).
37
38 [35] K. Palmo and S. Krimm, *Chem. Phys. Lett.*, **395**, 133 (2004).
39
40 [36] Beu, T.; Buck, U., *J. Chem. Phys.*, **2001**, 114, 7848.
41
42 [37] W. T. Vetterling and W. H. Press and S. A. Teukolski and B. P. Flannery, pp. 406, *Numerical Recipes*,
43 Cambridge University Press (Cambridge, 2001).
44
45
46
47
48
49
50
51
52
53
54
55
56
57
58
59
60

- 1
2
3 [38] Burnham, C. J.; Xantheas, S. S.; Miller, M. A.; Applegate, B. E.; Miller, R. E., *J. Chem. Phys.*, **2002**,
4 117, 1109.
5
6
7
8 [39] Greer, J. C.; Ahlrichs, R.; Hertel, I. V., *Chem. Phys. Lett.*, **1989**, 133, 191.
9
10 [40] A. N. Tharrington and K. D. Jordan, *J. Phys. Chem. A* **107**, 7380 (2003).
11
12 [41] A. Lenz and L. Ojamäe, *Phys. Chem. Chem. Phys.* **7**, 1905 (2005).
13
14 [42] Q. Shi, S. Kais, and J. S. Francisco, *J. Phys. Chem. A* **109**, 12036 (2005).
15
16
17
18
19
20
21
22
23
24
25
26
27
28
29
30
31
32
33
34
35
36
37
38
39
40
41
42
43
44
45
46
47
48
49
50
51
52
53
54
55
56
57
58
59
60

Figure captions:

Figure 1: Reference geometries and coordinates for the 2 dimensional CP-MP2/aug-cc-pVTZ scans. α generically indicates the angle employed in the 2D scans to explore the energy landscape of specific isomerization process.

Figure 2: Comparison between the original Model C (parameters and analytical form taken from Ref. [12]) and CP-MP2/aug-cc-pVTZ interaction energies (kcal/mol) as a function of the N–N distance (\AA). Panel a: linear (H-bonded) and parallel geometries. Panel b: mirror and bifurcated geometries.

Figure 3: Signed energy difference between *ab initio* and model potential interaction energies. Panel a: Model C with parameters and analytical form from Ref. [12]. Panel b: Model C(pol, Q^{frozen}). Panel c: Model C(pol, Q^{opt}).

Figure 4: Equilibrium geometries for the ammonia dimer obtained using CP-MP2/aug-pVTZ and Model C(pol, Q^{opt}) (in brackets, distances in \AA).

Figure 5: Structure of the putative global minima for $(\text{NH}_3)_n$ ($n=3-11$) optimized using Model C(pol, Q^{opt}).

Figure 6: Structure of the putative global minima for $(\text{NH}_3)_n$ ($n=12-20$) optimized using Model C(pol, Q^{opt}).

Figure 7: Local minimum structures obtained using Model C(pol, Q^{opt}) for some cluster size. a) “Butterfly” isomer for $(\text{NH}_3)_5$; b) Second energy isomer for $(\text{NH}_3)_6$; c) Second lowest energy isomer for $(\text{NH}_3)_8$; d) Second lowest energy isomer for $(\text{NH}_3)_{12}$.

Figure 8: Energy differences (cm^{-1}) from the global minimum of the lowest 200 isomers for $(\text{NH}_3)_n$ ($n=4-20$).

Figure 9: Evaporation energy ($E_n - E_{n-1}$, kcal/mol) for $(\text{NH}_3)_n$ computed using the total energy of putative global minima. Data obtained using Model C(pol, Q^{opt}); also showing the results provided in Ref. [36].

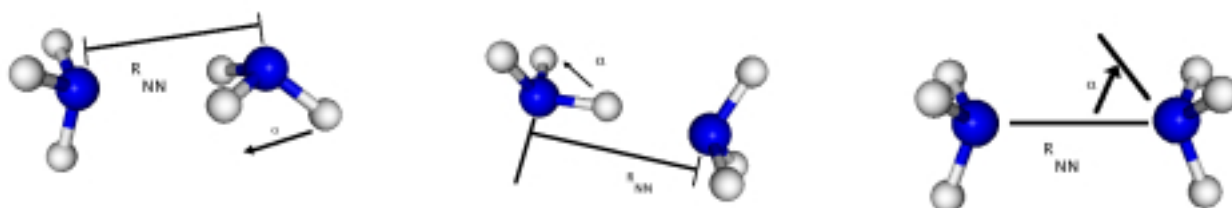


Figure 1: Mella

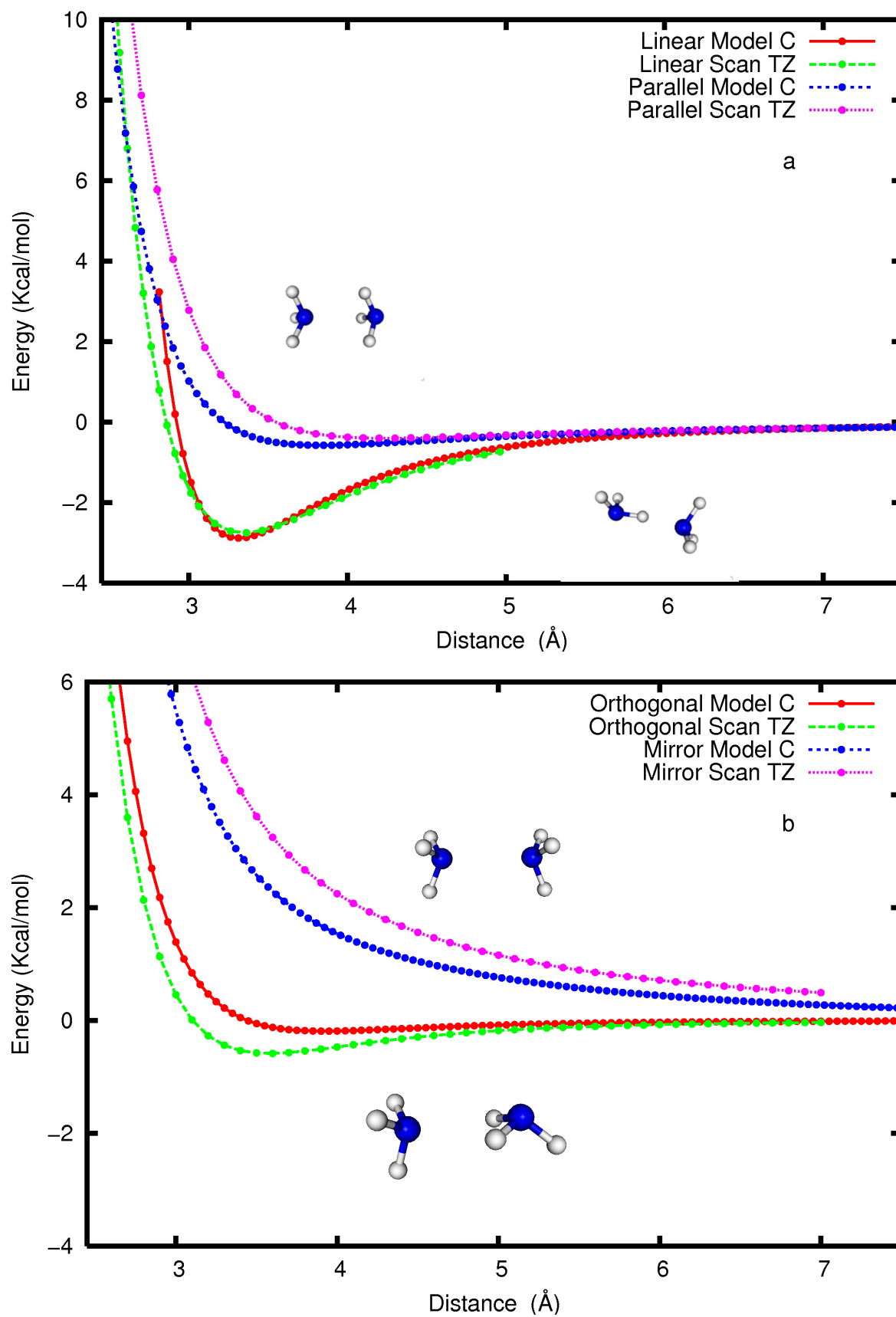
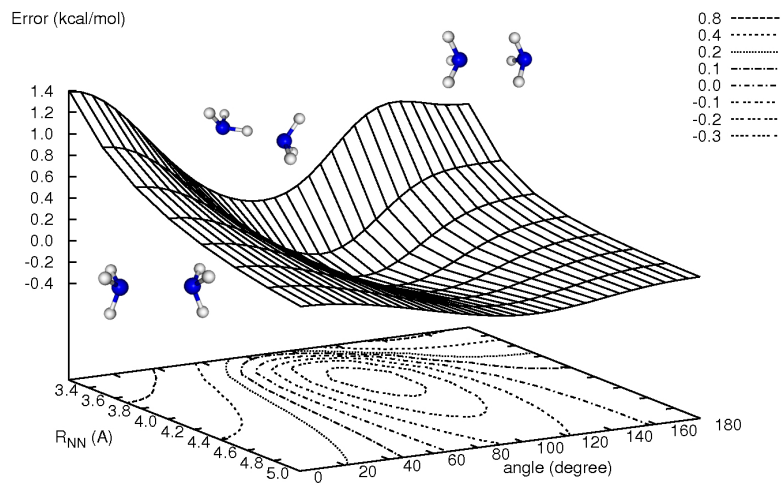
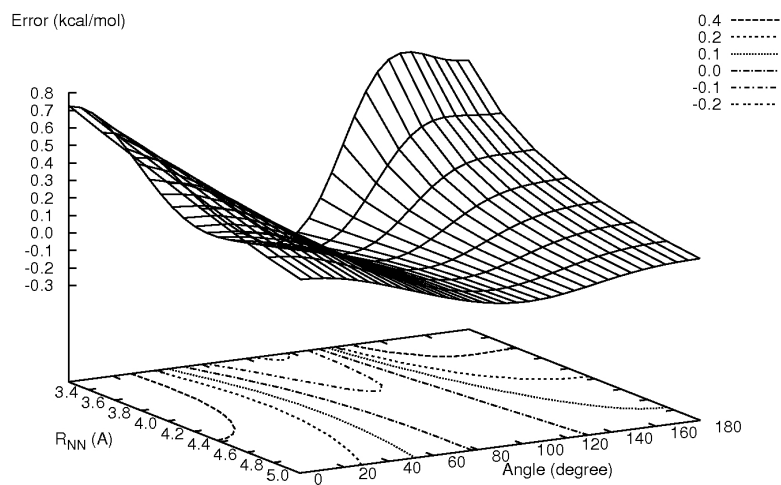


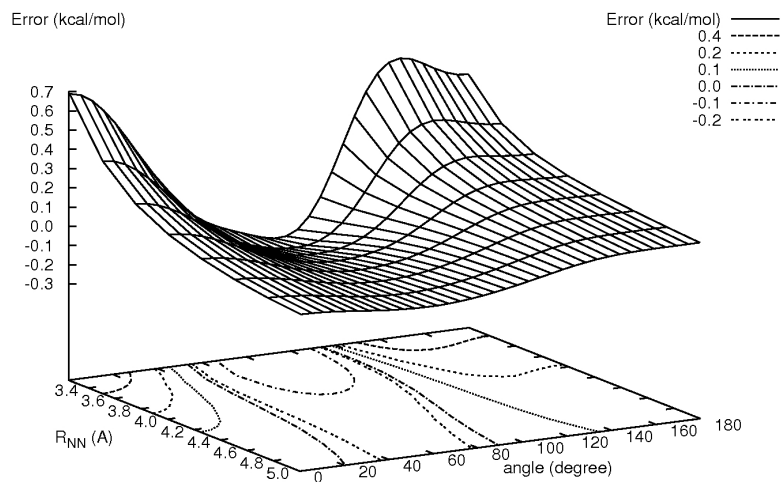
Figure 2: Mella



A



B



C

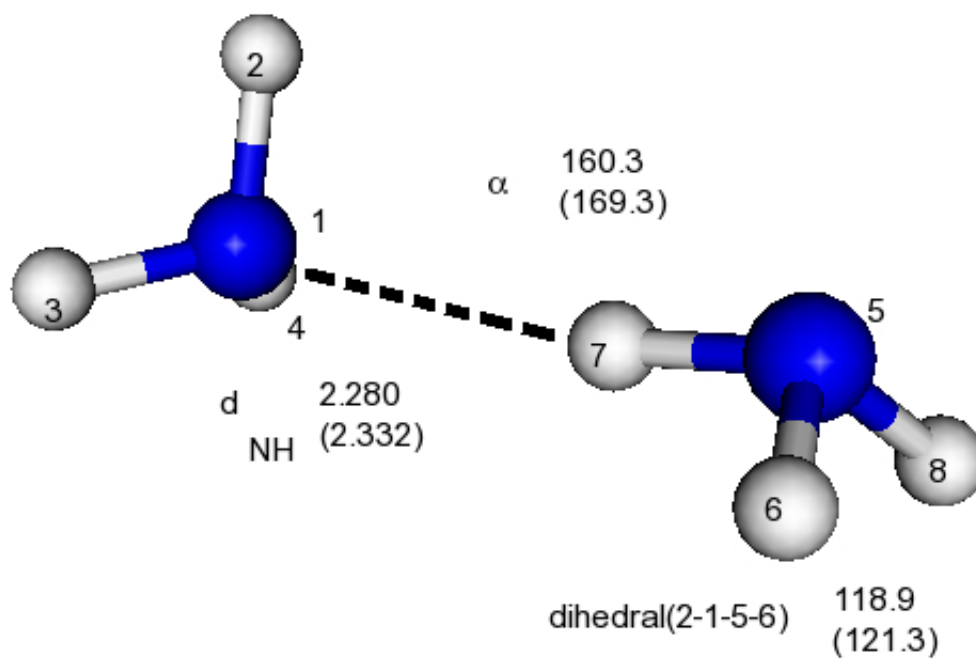


Figure 4: Mella

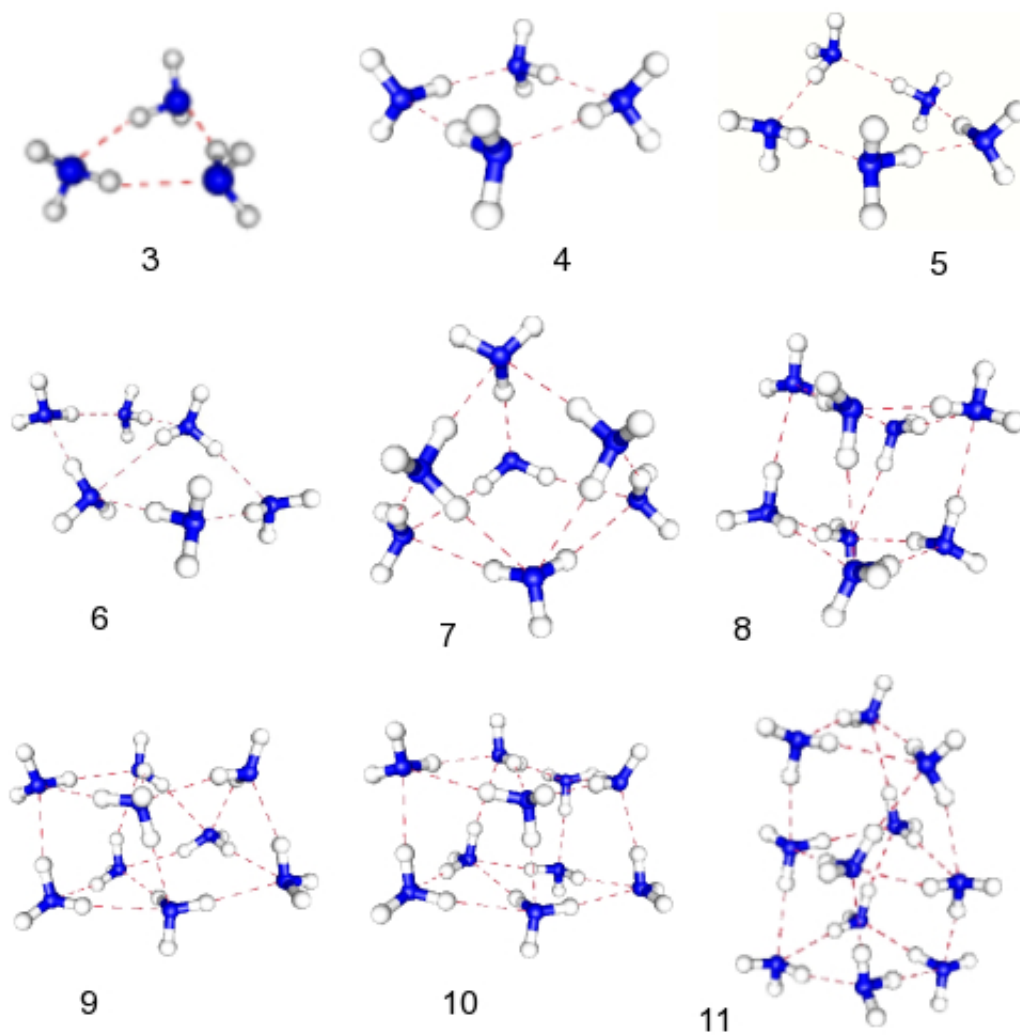


Figure 5: Mella

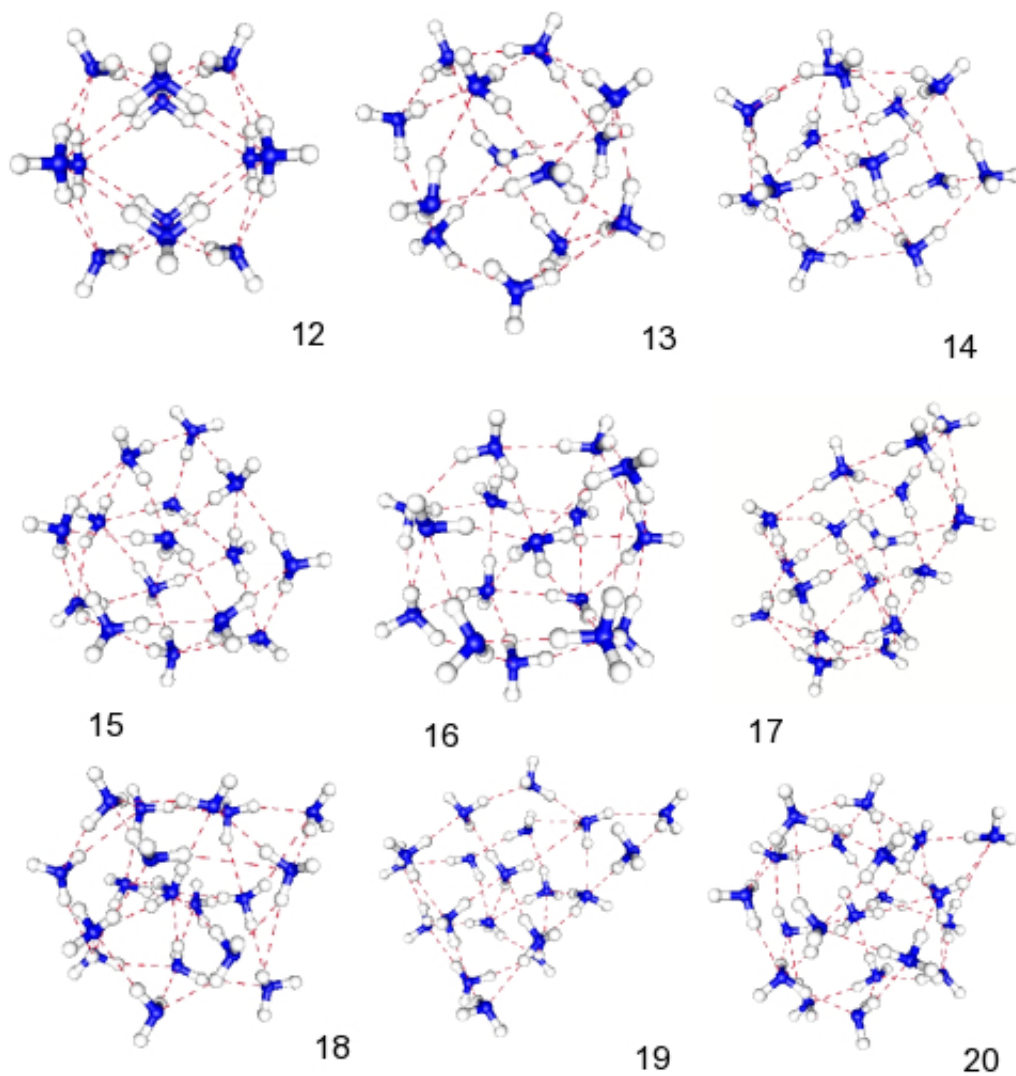


Figure 6: Mella

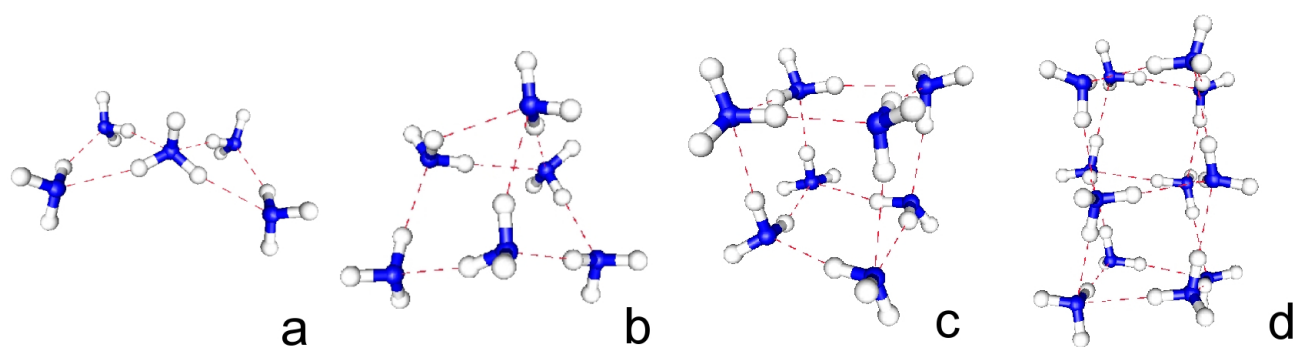


Figure 7: Mella

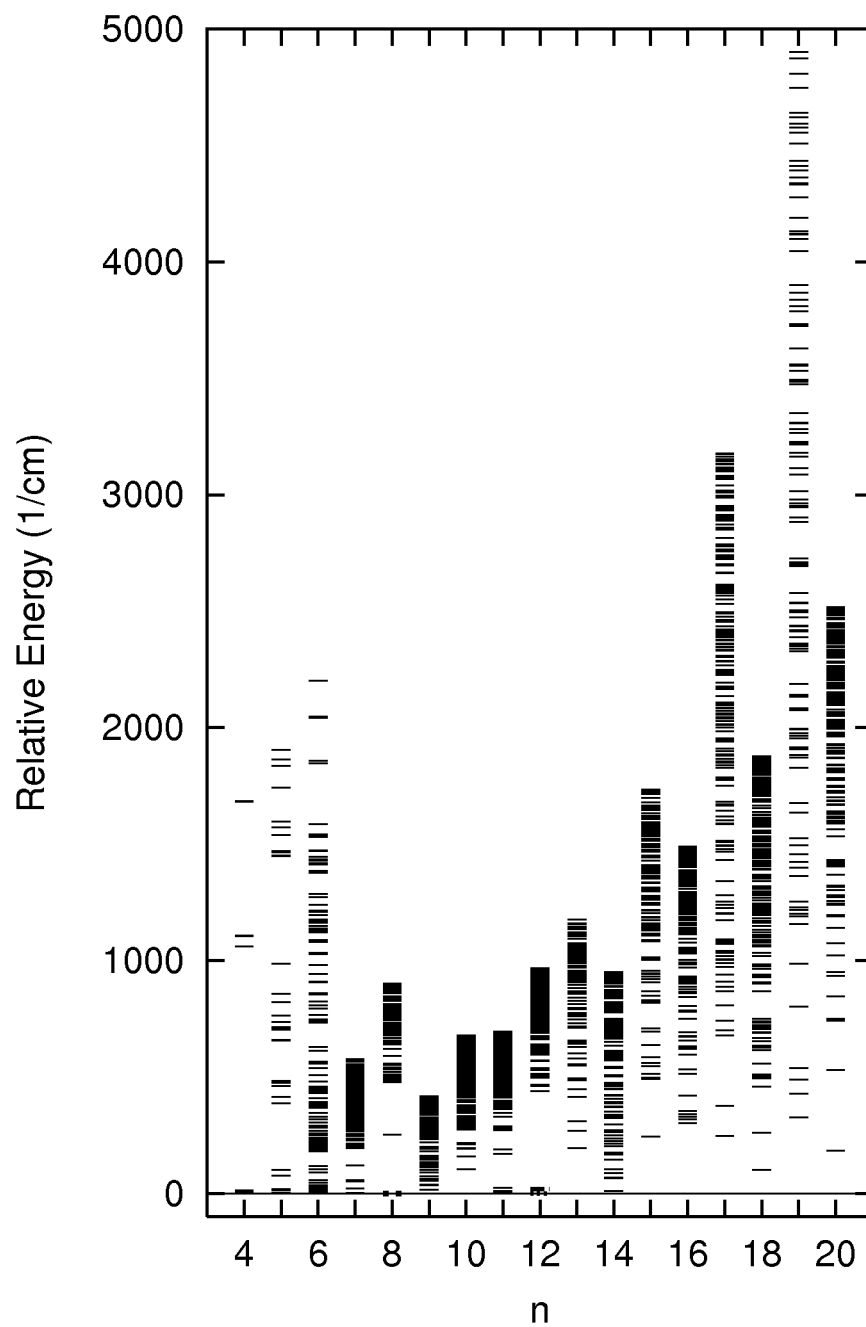


Figure 8: Mella

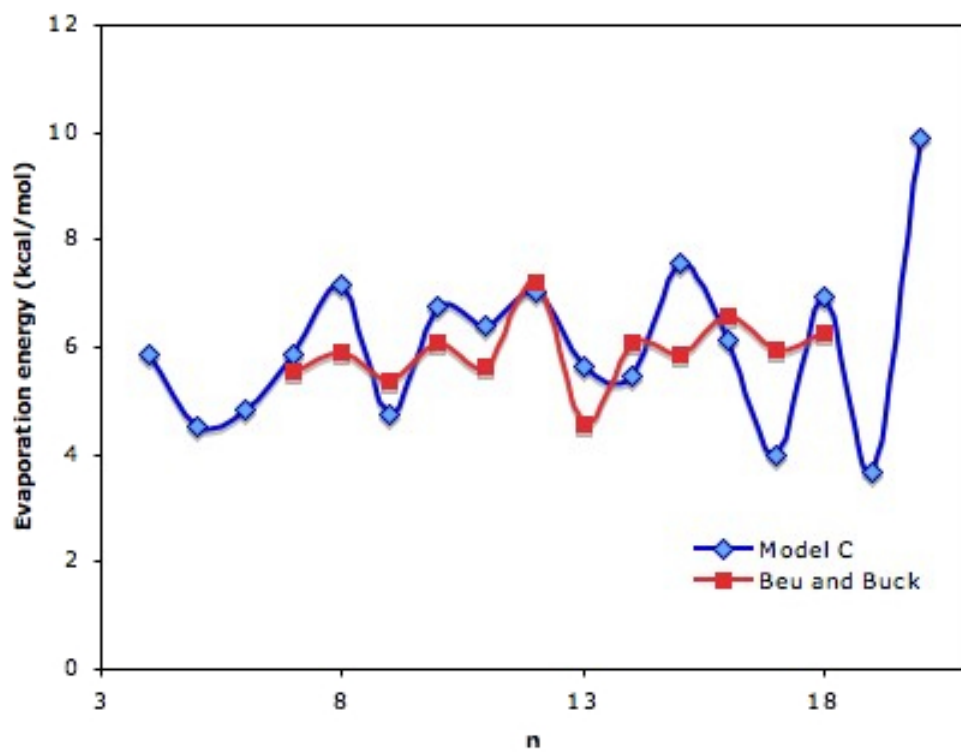


Figure 9: Mella